Cooperation of tissue factor cytoplasmic domain and PAR2 signaling in breast cancer development

Florence Schaffner,[1] Henri H. Versteeg,[1,2] Anja Schillert,[1] Naho Yokota,[1] Lars C. Petersen,[3] Barbara M. Mueller,[4] and Wolfram Ruf[1]

[1]Department of Immunology and Microbial Science, The Scripps Research Institute, La Jolla, CA; [2]Leiden University Medical Center, Leiden, The Netherlands; [3]Novo Nordisk, Malov, Denmark; and [4]Torrey Pines Institute for Molecular Studies, San Diego, CA

Constitutive expression of tissue factor (TF) by cancer cells triggers local activation of the coagulation cascade and promotes breast cancer progression through cell signaling involving protease activated receptor (PAR)2. In human breast cancer, TF and PAR2 are up-regulated and TF cytoplasmic domain phosphorylation is correlated with relapse. Here we show that cancer cell PAR2 signaling promotes angiogenesis independent of PAR2 phosphorylation at the recognized β-arrestin recruitment site. Similar to PAR2$^{-/-}$ mice, TF cytoplasmic domain–deleted (TF$^{\Delta CT}$) mice have delayed spontaneous breast cancer development in the polyoma middle T model. Simultaneous deletion of PAR2 in TF$^{\Delta CT}$ mice did not further delay tumor appearance, consistent with overlapping roles of TF and PAR2 in promoting the angiogenic switch in early stages of breast cancer. In advanced carcinomas, tumor-associated macrophages were reduced in TF$^{\Delta CT}$ and TF$^{\Delta CT}$/PAR2$^{-/-}$ mice, and increased tumor vessel diameters of TF$^{\Delta CT}$ mice were partially reversed by PAR2-deficiency, indicating that the TF cytoplasmic domain has additional roles that are interdependent with PAR2 signaling in regulating host angiogenic responses. These experiments demonstrate a crosstalk of tumor cell TF cytoplasmic domain and PAR2 signaling and provide a possible mechanism for the close correlation between TF phosphorylation and cancer recurrence of TF and PAR2-positive clinical breast cancer. (*Blood*. 2010;116(26): 6106-6113)

Introduction

Local and systemic coagulation activation is a hallmark of advanced malignancies.[1,2] Cancer cell–expressed tissue factor (TF) is a major procoagulant stimulus in cancer-associated thrombosis, and tumor cell TF expression is correlated with tumor progression in several experimental tumor models (reviewed in Schaffner and Ruf[3]). Although thrombin generated in the course of coagulation supports hematogenous metastasis[4] and regulates angiogenesis and the tumor microenvironment,[5] several lines of pharmacological and genetic evidence show that direct signaling of TF plays a pivotal role in cancer progression and angiogenesis.

The TF-VIIa complex cleaves the G protein-coupled protease activated receptor (PAR) 2[6] and triggers breast cancer cells to produce a diverse repertoire of angiogenic regulators and immune-modulatory cytokines.[7-9] The cleavage of PAR2 activates Gαq, Gα12/13, and Gαi, and termination of signaling occurs upon internalization of the receptor that is initiated by the binding of β-arrestins to phosphorylated residues on the C-terminus of G protein–coupled receptors. β-arrestins also promote G-protein independent signaling by serving as a scaffold for activating the extracellular regulated kinases (ERK) pathway.[10] The coupling of β-arrestin to PAR2 results in the dephosphorylation of cofilin, which leads to the severing of actin filaments.[11] Thus, the activation of the noncanonical pathway through β-arrestin promotes breast cancer motility.[11-14]

The TF-VIIa–signaling complex is associated with integrins and regulates α3β1-dependent migration in a crosstalk that involves the TF cytoplasmic domain in noncancerous epithelial cells.[15] In cancer cells, TF is constitutively associated with β1 integrins that regulate TF-VIIa-PAR2–mediated induction of proangiogenic chemokines.[16] Importantly, a unique monoclonal antibody to human TF without significant anticoagulant properties specifically disrupts the interaction of TF with integrins, TF-VIIa-PAR2 cell signaling, and the growth of human breast cancer xenografts in mice,[16] demonstrating that TF-PAR2 signaling is a potential therapeutic target for cancer therapy.

Although breast cancer cell PAR1 signaling is deregulated to increase invasiveness[17,18] and is partially overlapping with TF-PAR2 signaling in promoting transcriptional responses,[8] only PAR2 deficiency significantly delays the progression from adenoma to adenocarcinoma in the polyoma middle T (PyMT) model of spontaneous breast cancer development.[19] In this mouse model, the oncogenic middle T-antigen protein is expressed under a mammary-specific promoter, and mice expressing the transgene develop tumors in all mammary glands. Tumor progression resembles the human disease[20] at the molecular level (eg, down-regulation of the estrogen and progesterone receptors) and, due to the relatively slow development, allows the study of complex interactions between the host and tumor cells. Because postnatal, hypoxia-induced and transplanted tumor angiogenesis is unaffected in PAR1$^{-/-}$ or PAR2$^{-/-}$ mice,[19,21] the delayed vascularization of PyMT/PAR2$^{-/-}$ tumors is most consistent with impaired tumor cell proangiogenic signaling. Accordingly, blocking TF-PAR2 signaling specifically on tumor cells reduces microvessel density in xenograft tumors.[16] In the present study, reconstitution experiments

in PyMT PAR2^{−/−} breast cancer cells directly show that tumor cell PAR2 signaling supports tumor growth and angiogenesis.

TF is expressed by multiple cell types in the tumor microenvironment, including tumor-associated macrophages, endothelial cells, and fibroblasts.[3] Host cell–derived TF makes independent contributions to tumor development of transplanted teratomas,[22] and in models of hypoxia-induced angiogenesis, TF cytoplasmic domain–deleted mice (TF[ΔCT] mice) display accelerated angiogenesis, a phenotype that is reversed by simultaneous deficiency in PAR2.[23] Although the TF cytoplasmic domain has been implicated in the growth of certain tumors[24] and hematogenous tumor dissemination,[25,26] it is unknown whether signaling of the TF cytoplasmic domain is restricted to the host compartment in breast cancer progression. Clinical breast cancer biopsies show a marked up-regulation of both PAR2 and TF antigen in invasive tumor cells.[27] PAR2 activation induces TF cytoplasmic domain phosphorylation,[28] and TF phosphorylation is detectable in wild-type (WT), but not PAR2^{−/−} PyMT, tumor cells. Remarkably, phosphorylation of the TF cytoplasmic domain is also detectable in clinical breast cancer samples and correlated with breast cancer relapse.[27] Considering these clinical findings, we set out to characterize the contributions of the TF cytoplasmic domain to spontaneous breast cancer development in the PyMT model. These experiments in PyMT TF[ΔCT] and PyMT TF[ΔCT]/PAR2^{−/−} double-deficient mice provide new insight into the interplay of TF cytoplasmic domain and PAR2 signaling in breast cancer cell and host angiogenic responses.

Methods

Mice

PyMT C57BL/6 WT, PyMT C57BL/6 TF[ΔCT], and C57BL/6 TF[ΔCT]/PAR2^{−/−} mice were generated by crossing with C57BL/6 PyMT mice.[19] Cohorts of PyMT-WT, TF[ΔCT], and TF[ΔCT]/PAR2^{−/−} mice were monitored weekly for tumor appearance and sizes of mammary glands. Tumor volumes were calculated using the formula $v = 0.5*(length \times width^2)$. Mice were killed when the size of the largest tumor exceeded institutional guidelines. Tumors and lungs were harvested and either fixed in Zinc fixative for immunohistochemistry or snap frozen for RNA extraction. Lung metastases were quantified as described.[19] All animal experiments were performed under approved protocols of the The Scripps Research Institute Institutional Animal Care and Use Committee.

Generation of PAR2-replete tumor cells

PAR2^{−/−} mammary carcinoma cells established from PyMT-PAR2^{−/−} mice[19] were in vivo selected once in the mammary fat pad and used after re-isolation at early passages for reconstitution experiments. PAR2^{−/−} cells were transduced with either the control virus encoding the DS-Red fluorescent protein (Mock) or the virus expressing either mouse WT PAR2 (PAR2[WT]) or PAR2[Ser365Ala] (PAR2[ΔARR]), which lacks the phosphorylation site required for β-arrestin binding.[29] Transduction efficiency was quantified by measuring DS-Red fluorescence by flow cytometry.

Signaling assays

Mock, PAR2[WT], or PAR2[ΔARR] cells were plated and serum-deprived for 24 hours. Cells were then stimulated with the PAR2 agonist peptide SLIGRL (100μM), trypsin (10nM), murine VIIa (5nM),[30] or the ternary TF coagulation initiation complex (VIIa [5nM], X [50nM], and nematode anticoagulant protein c2 [NAPc2, 200nM]) for 90 minutes. All reactions included hirudin (200nM) when coagulation proteases were present to prevent thrombin effects. Induction of mRNA levels was quantified by reverse transcription polymerase chain reaction as described.[19]

Flow cytometric analysis

Mock, PAR2[WT], or PAR2[ΔARR] cells were harvested with trypsin. The cells were stained with fluorophore-conjugated monoclonal rat anti–mouse TF antibody 11F6 for 30 minutes on ice.[27] This antibody was generated in the laboratory against recombinant mouse TF extracellular domain and confirmed to be nonreactive with TF-negative mouse tumor cells. After 2 washes with phosphate-buffered saline (PBS)/fetal calf serum (FCS) 2%/1mM EDTA (ethylenediaminetetraacetic acid), the cells were fixed with 1% paraformaldehyde (PFA). Flow cytometric results were analyzed with FlowJo 8 (TreeStar).

Orthotopic tumor growth

Mock, PAR2[WT], or PAR2[ΔARR] cells (5×10^5 cells in 50 μL of serum-free medium) were injected into the second left mammary gland of female C57BL6/J mice. Tumor volumes were measured twice weekly with a caliper, as described in the first paragraph. When tumors reached institutional size limits, mice were killed, tumor weights were determined, and tumors were fixed in Zinc fixative for histology.

Histology

Fixed tumors were embedded in paraffin. Tumor sections (5 μm) were deparaffinized in xylene and rehydrated in alcohol. Sections were blocked with 5% bovine serum albumin (BSA)/0.2% Tween-20 for 1 hour and stained overnight in the cold with primary anti-CD31 (BD Biosciences), specific for murine endothelial cells, or anti-F4/80 (Caltag), a macrophage marker, or anti–platelet-derived growth factor receptor (PDGFR)–β (eBioscience). Specific biotinylated secondary antibody (Vector Laboratories) was added for 1 hour, and staining was visualized with either avidin-biotin-peroxidase complex (ABC) reagent using 3,3-diaminobenzidine to develop horseradish peroxidase or Alexa-488 conjugated to streptavidin (Molecular Probes). Sections were counterstained with either hematoxylin and then dehydrated and mounted in Permount (Fisher Scientific) embedding medium or with DAPI (4,6 diamidino-2-phenylindole) and mounted with fluorescent medium (Dako). Phospho-histone H3 (Cell Signaling Technology) staining used paraffin sections that were deparaffinized in xylene and rehydrated in alcohol. Sections were boiled in citrate buffer pH 6 for 10 minutes, blocked with Tris (tris(hydroxymethyl)aminomethane)–buffered saline (TBS)/5% goat serum for 1 hour, and reacted with anti–phospho-histone H3 overnight in the cold. Primary antibody was detected with biotinylated anti–rabbit antibody followed by Alexa-546–conjugated streptavidin and DAPI counterstaining of nuclei in fluorescent mounting medium. Masson trichrome staining was performed according to the manufacturer's protocol (Sigma-Aldrich). Tumor grading was performed blindly according to Lin et al.[20]

A Nikon laboshot microscope with 6.3×/0.2 or 16×/0.4 objectives and Qimagig, FAST 1394 was used for Masson and F4/80 imaging. Images were then processed with Photoshop CS4. For microvessel density, pericyte coverage, and phospho histone 3 quantification, a Zeiss LSM 710 laser scanning confocal microscope with 40× oil-PlanNeoFluor-1.3na objective and Zen 2009 software were used. Vessel counts were quantified with the Imaris Version 7 software (BitPlane Inc) in at least 4 randomly chosen fields from each tumor specimen. Tumor and vessel areas were quantified with Image Pro Plus 7 (Media Cybernetics Inc) as described.[31] In the trichrome staining, the hematoxylin and eosin staining was used to define tumor area. For fibrotic tumors, the blue collagen staining was removed from the quantification of tumor areas by adjusting the threshold. Colocalization of CD31 and PDGFR-β staining was quantified with Imaris.

Statistical analysis

A log rank test was performed to establish differences in tumor appearance (Prism Version 5, GraphPad Software). Analysis of variance (ANOVA) followed by t test was performed to compare groups, and $P < .05$ was
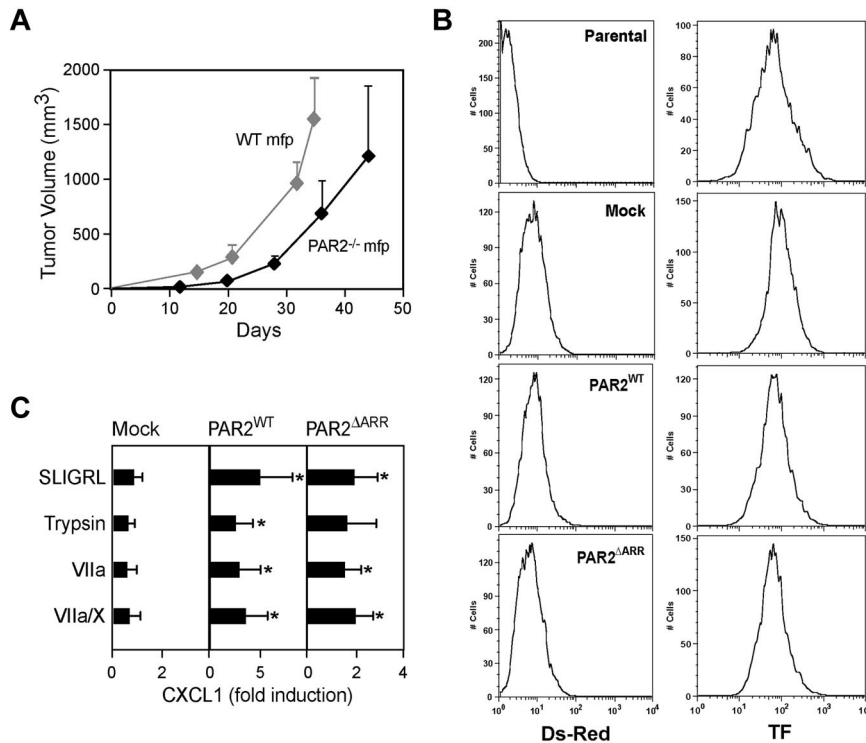
Figure 1. Reconstitution of PAR2 signaling in PAR2$^{-/-}$ PyMT breast cancer cells. (A) Growth properties of PyMT WT and PAR2$^{-/-}$ breast cancer cells after in vivo passage through the mammary fat pad (n = 8 mice/group, representative of at least 2 experiments). (B-C) PyMT PAR2$^{-/-}$ cells were transduced twice with control (Mock), PAR2^{WT}, or PAR2$^{\Delta ARR}$ retrovirus. (B) Quantification of transduction efficiency was determined by flow cytometry measuring DS-Red fluorescence. PAR2-reconstitution did not change TF cell surface expression. (C) PAR2 reconstitution restores CXCL1 induction by PAR2 agonist SLIGRL (100μM), trypsin (10nM), VIIa (5nM), or the ternary complex (VIIa (5nM), X (50nM), nematode anticoagulant protein c2 (200nM)). Hirudin (200nM) was added to all reactions that included coagulation factors. CXCL1 induction was assessed by quantitative reverse transcription polymerase chain reaction after 90 minutes of stimulation. Means and ± SD, n = 4; * $P < .05$ different from mock-transduced cells by ANOVA.

considered as a significant difference. The χ^2 analysis of goodness of fit was used to evaluate histological differences in tumor progression, as described.[19]

Results

PAR2 reconstitution of PyMT PAR2$^{-/-}$ cells restores aggressive tumor growth and increases tumor angiogenesis

We had previously isolated PyMT PAR2$^{-/-}$ breast cancer cells that showed reduced subcutaneous tumor growth at the same cell dose as WT counterparts in either WT or PAR2$^{-/-}$ host mice.[19] Tumor growth experiments with PyMT WT and PAR2$^{-/-}$ cells placed into the mammary fat pad confirmed reduced aggressiveness of PyMT PAR2$^{-/-}$ cells in the orthotopic tumor microenvironment (Figure 1A). All subsequent experiments were carried out with tumor cell populations that were adapted by in vivo passages through the mammary fat pad. Tumor cell TF-VIIa-PAR2 signaling induces proangiogenic cytokines[8,9,16] or promotes breast cancer motility through β-arrestin recruitment.[12,13] We therefore reconstituted PyMT PAR2$^{-/-}$ cells with murine WT PAR2 (PAR2^{WT}) or a single amino-acid (Ser^{365} to Ala) replacement mutant of murine PAR2 (PAR2$^{\Delta ARR}$) that lacked a conserved protein kinase C (PKC) phosphorylation site. This site was previously shown to mediate β-arrestin recruitment and G protein–independent ERK1/2 scaffolding of human PAR2,[29] although presumably G protein–coupled receptor kinase–mediated phosphorylation of the Ser-rich carboxyl terminus of PAR2 also contributes to arrestin binding.[32]

PAR2 was delivered with retroviral constructs that coexpressed the DS-Red fluorescent protein for direct monitoring of transduction efficiency. Equivalent reconstitution with PAR2 or PAR2$^{\Delta ARR}$ had no effect on the cell surface expression of TF, excluding major phenotypic changes after the restoration of PAR2 signaling (Figure 1B). PAR2-dependent induction of the proangiogenic cytokine CXCL1 by the PAR2 agonist peptide SLIGRL (Figure 1C) was efficiently restored by transduction with both PAR2^{WT} and PAR2$^{\Delta ARR}$. CXCL1 was also induced after proteolytic cleavage of PAR2 with trypsin, TF-VIIa, or the ternary TF-VIIa-Xa complex, indicating that PAR2 is cell surface–expressed and accessible to extracellular proteases.

Orthotopic tumor growth of mock-, PAR2^{WT}-, or PAR2$^{\Delta ARR}$-transduced cells was characterized in 3 independent experiments. A typical tumor growth curve is shown in Figure 2A and the final tumor volumes for each experiment are shown in Figure 2B. Reconstitution with either PAR2^{WT} or PAR2$^{\Delta ARR}$ reproducibly enhanced tumor growth in the mammary fat pad, indicating that the restoration of proangiogenic chemokine induction was sufficient for a more aggressive tumor growth phenotype of PAR2-replete cells. Vessel density of end-stage tumors confirmed the expected enhanced angiogenesis in PAR2-replete cells (Figure 2C). We also assessed macrophage density and the proliferative index in tumors and found no differences between PAR2^{WT}-, PAR2$^{\Delta ARR}$-, or mock-transduced tumors (Figure 2D-E). These data directly showed that tumor cell PAR2 signaling promotes angiogenesis and excluded that PKC-dependent β-arrestin recruitment[29] was required for PAR2-dependent breast cancer growth.

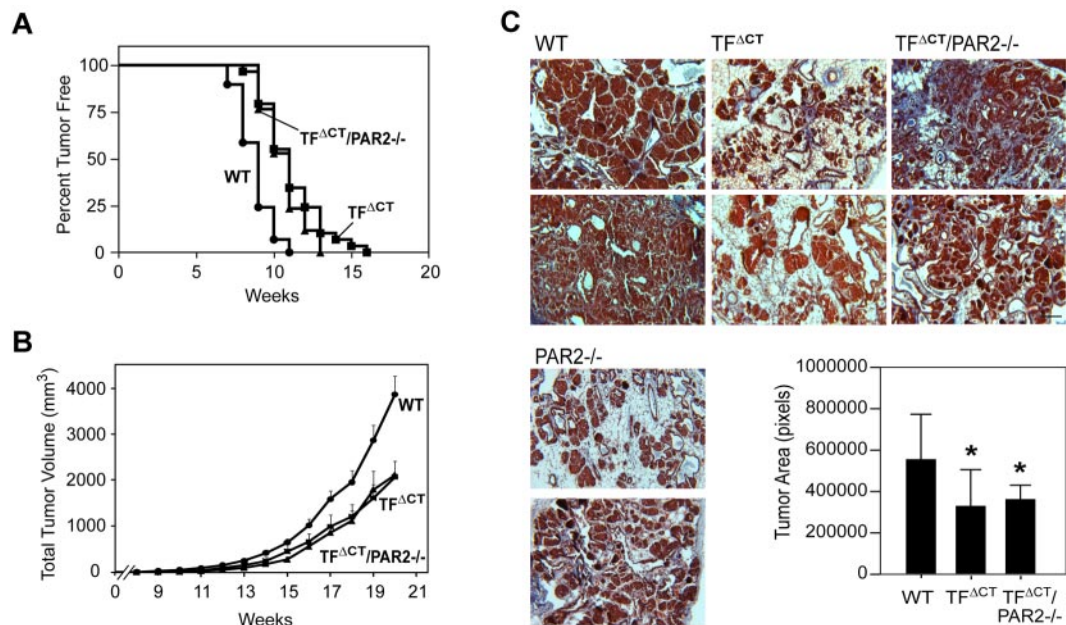## Delayed spontaneous breast cancer development in TF$^{\Delta CT}$ mice

In the PyMT model, PAR2$^{-/-}$ mice displayed a delayed appearance of palpable breast tumors and concordant histological findings of slower progression from adenoma to invasive carcinoma in early-stage tumor development.[19] To address if the TF cytoplasmic domain is linked to PAR2 signaling, as suggested by the phospho TF staining in preclinical and clinical samples,[27] cohorts of PyMT TF$^{\Delta CT}$ and PyMT TF$^{\Delta CT}$/PAR2$^{-/-}$ mice were followed. The appearance of palpable tumors was significantly delayed from a mean of 9 weeks for PyMT C57BL/6 WT controls to 11 weeks for PyMT TF$^{\Delta CT}$ and PyMT TF$^{\Delta CT}$/PAR2$^{-/-}$ (Figure 3A). Tumor
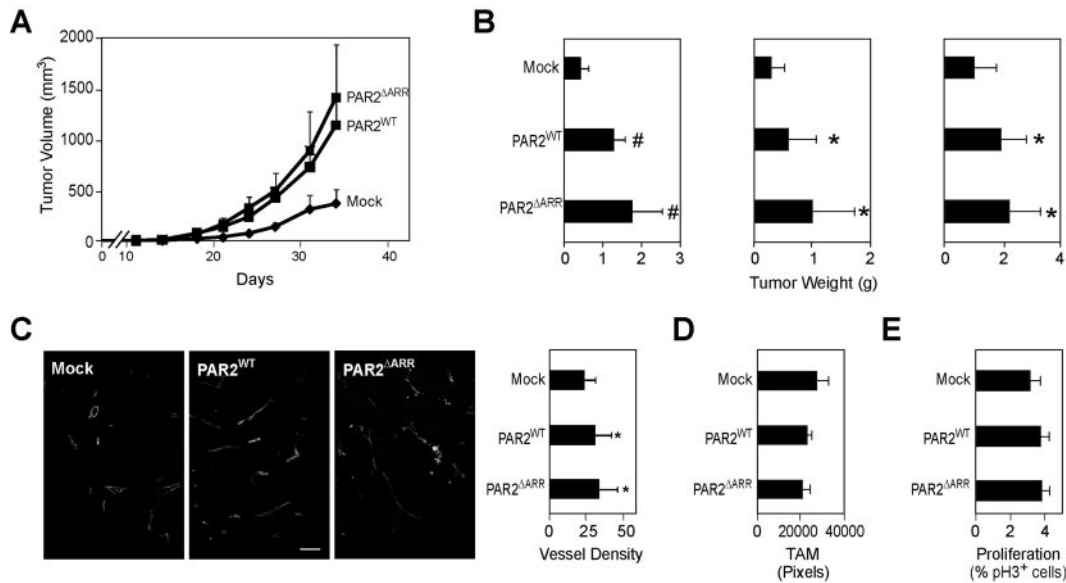
Figure 2. Breast Cancer PAR2 signaling promotes tumor growth and angiogenesis. (A) Typical experiment of orthotopic tumor growth of C57BL/6 mammary fat pad implanted mock, PAR2^WT, or PAR2^ΔARR transduced PyMT PAR2^−/− breast cancer cells (5×10^5/mouse). Tumor volumes are mean ± SD, n ≥ 7 mice/group, $P < .05$ different from mock by ANOVA. (B) Final tumor weights from 3 independent experiments, mean ± SD, n ≥ 7 mice/group, *$P < .05$; #$P < .001$ different from mock by ANOVA. (C) Vessel density of mock, PAR2^WT, or PAR2^ΔARR tumors was determined on fixed sections stained with CD31. Tumor vessels were quantified with the IMARIS software in at least 4 different areas per tumor, and at least 4 mice/genotypes were analyzed, mean ± SD, * different from mock tumors, $P < .05$, ANOVA, scale bar 50 μm. (D) Tumor macrophage density was quantified in 4 fields per tumor (n ≥ 3, mean + SEM, $P = .5$ ANOVA). (E) Phospho Histone 3 and DAPI staining were quantified in at least 4 fields of view with the IMARIS software (n ≥ 4, mean ± SEM, $P = .4$ ANOVA).

burden remained lower throughout the observation period for both PyMT TF^ΔCT and PyMT TF^ΔCT/PAR2^−/− mice (Figure 3B). Blinded tumor staging of 17 PyMT WT, 17 PyMT TF^ΔCT and 11 PyMT TF^ΔCT/PAR2^−/− mice at 11-13 weeks of age showed more advanced disease in WT versus knock-out mice. Hyperplasia or absence of visible tumors in all glands were more prevalent in PyMT TF^ΔCT (82%) and PyMT TF^ΔCT/PAR2^−/− (54%) mice than in WT (23%) mice, whereas WT had progressed to the adenoma (53%) and invasive adenocarcinoma (24%) stage significantly more than PyMT TF^ΔCT (18/0%) and PyMT TF^ΔCT/PAR2^−/− (27/18%) mice (χ^2 analysis $P < .001$ WT vs TF^ΔCT, $P = .009$ WT vs TF^ΔCT/PAR2^−/−).

Figure 3. TF cytoplasmic domain deletion impairs spontaneous breast cancer development in the PyMT model. (A) Cohorts of 29 PyMT WT, 29 PyMT TF^ΔCT, and 17 PyMT TF^ΔCT/PAR2^−/− mice were examined weekly for palpable tumors and tumor incidence was recorded. The mean time for appearance was delayed from 9 weeks for WT to 11 weeks for PyMT TF^ΔCT, and TF^ΔCT/PAR2^−/− mice ($P < .0001$ log-rank test). (B) Cumulative tumor burden was determined by weekly measurements of tumor volumes in all mammary glands. PyMT TF^ΔCT and TF^ΔCT/PAR2^−/− mice had reduced tumor masses relative to WT, mean ± SEM, $P < .001$ ANOVA Kruskal-Wallis. (C) Tumor progression in 11-13-week-old mice. Detectable tumors were harvested with a similar age distribution in each group. Fixed tumor sections were stained with Masson trichrome and tumor areas were quantified with Image Pro Plus. Tumor areas were smaller in PyMT TF^ΔCT and TF^ΔCT/PAR2^−/− relative to WT, n ≥ 10, mean ± SD, $P < .05$ ANOVA. Representative images, scale bar is 100 μm.

The initial evaluation of hematoxylin and eosin (H&E)–stained sections of early (11-13 weeks) tumors suggested larger tumor areas in a subpopulation (approximately 40%) of TF$^{\Delta CT}$/PAR2$^{-/-}$ mice relative to TF$^{\Delta CT}$ mice. However, Masson trichome staining revealed increased extracellular matrix deposition in this subset of TF$^{\Delta CT}$/PAR2$^{-/-}$ tumors (Figure 3C). Staining of 6 independent PyMT PAR2$^{-/-}$ tumors did not detect a similar fibrotic response (Figure 3C), indicating a phenotype that is unique to the PyMT TF$^{\Delta CT}$/PAR2$^{-/-}$ strain. Furthermore, tumors of all strains at late stages showed extracellular matrix deposition, the extent of which was not appreciably different between tumors isolated from PyMT WT, TF$^{\Delta CT}$, PAR2$^{-/-}$, and TF$^{\Delta CT}$/PAR2$^{-/-}$ mice (data not shown).

Trichome-stained sections allowed for quantitative image analysis of tumor-cell areas that at 11-13 weeks showed significantly decreased tumor sizes for both PyMT TF$^{\Delta CT}$ and PyMT TF$^{\Delta CT}$/PAR2$^{-/-}$ mice relative to WT controls (Figure 3C). Thus, TF cytoplasmic domain deletion and PAR2-deficiency produced a comparable and nonadditive effect in delaying the early steps of spontaneous tumor development in the PyMT model. Similar to previous transplanted tumor growth experiments in PAR2$^{-/-}$ mice,[19] PyMT WT breast cancer cells grew indistinguishable in the mammary fat pad of WT or TF$^{\Delta CT}$ host mice (2 independent experiments, data not shown), indicating that tumor cell signaling was mainly responsible for the delayed tumor appearance in PyMT TF$^{\Delta CT}$ mice.

In a heterologous expression model in Chinese hamster ovary (CHO) cells the cytoplasmic domain of TF supports efficient metastasis,[25] but other tumor models metastasize independent of the TF cytoplasmic domain.[33] The large variability of lung metastases in PyMT mice yielded no statistically significant differences, and potential roles of TF cytoplasmic domain and PAR2 signaling in metastasis require additional studies in more robust metastasis models.

Distinct effects of TF cytoplasmic domain deletion and PAR2-deficiency in late-stage PyMT tumors

In the previous characterization of late-stage PyMT PAR2$^{-/-}$ tumors, we found no differences in vessel density or macrophage counts.[19] Considering that the TF cytoplasmic domain influences macrophage signaling[34,35] and host angiogenic responses,[23] a more extensive evaluation of late stage tumors was performed. Late-stage PyMT TF$^{\Delta CT}$ tumors showed significantly larger tumor vessel diameter, based on quantitative image analysis of CD31-stained sections (Figure 4A-B). In contrast to the very similar phenotype of delayed early-stage tumor development in PyMT TF$^{\Delta CT}$ mice and PyMT TF$^{\Delta CT}$/PAR2$^{-/-}$ mice, vessel diameters were more heterogeneous in late-stage PyMT TF$^{\Delta CT}$/PAR2$^{-/-}$ tumors. Vessel diameters ranged from those observed in WT to the enlarged vessel sizes of PyMT TF$^{\Delta CT}$ mice (Figure 4A). Vessel diameter was also assessed in 5 PyMT PAR2$^{-/-}$ tumors, and only 1 of them displayed somewhat larger vessels. Masson trichrome staining showed no appreciable heterogeneity in extracellular matrix depositions for PyMT TF$^{\Delta CT}$/PAR2$^{-/-}$ tumors (data not shown), indicating that the diverse late-stage tumor vessel appearance was unrelated to this unique feature observed in a subset of early PyMT TF$^{\Delta CT}$/PAR2$^{-/-}$ tumors.

The vessels of PyMT TF$^{\Delta CT}$ and PyMT TF$^{\Delta CT}$/PAR2$^{-/-}$ mice also displayed decreased coverage by pericytes compared with WT, as evaluated by anti-PDGFRβ staining, but PyMT PAR2$^{-/-}$ tumors were indistinguishable from WT in this respect (Figure 4C).

Notably, the recruitment of F4/80$^+$ macrophages was substantially reduced in PyMT TF$^{\Delta CT}$ and TF$^{\Delta CT}$/PAR2$^{-/-}$ tumors versus PyMT WT or PyMT PAR2$^{-/-}$ tumors (Figure 4D-E). Thus, early PyMT tumor development in TF$^{\Delta CT}$, PAR2$^{-/-}$, and TF$^{\Delta CT}$/PAR2$^{-/-}$ mice is delayed similarly, but TF cytoplasmic domain deletion and PAR2-deficiency produce different vessel phenotypes in late stage tumors, possibly originating from signaling in the host macrophage compartment.

Discussion

TF is part of the tumor cell genetic program that is induced by multiple oncogenic transformation events during cancer progression,[36] but it remains incompletely understood how the embedding in cancer cell–signaling networks contributes to TF's partially overlapping roles in supporting angiogenesis and the tumor microenvironment.[19,23] Recent data from experimental tumor models and primary clinical breast cancer demonstrated a close correlation of cancer relapse, PAR2 expression, and phosphorylation of the TF cytoplasmic domain.[27] Here we provide evidence that these associations are not merely correlative, but rather have functional implication for breast cancer development in vivo.

In the PyMT model, the deletion of the TF cytoplasmic domain phenocopied the delayed tumor progression of PAR2$^{-/-}$ mice[19] and the similar phenotype of double-deficient TF$^{\Delta CT}$/PAR2$^{-/-}$ mice further link TF and PAR2 signaling in the spontaneous development of invasive breast cancer. In early stages of this model, PyMT PAR2$^{-/-}$, TF$^{\Delta CT}$, and TF$^{\Delta CT}$/PAR2$^{-/-}$ mice are characterized by a persistence of adenoma and a delayed development of invasive carcinoma that is dependent on the angiogenic switch.[20] Reconstitution experiments with PyMT PAR2$^{-/-}$ cancer cells further directly show that autonomous tumor cell PAR2 signaling promotes angiogenesis. By mutagenesis, we delineate that proangiogenic PAR2 signaling is independent of β-arrestin–dependent ERK1/2 scaffolding that requires phosphorylation of a conserved PKC phosphorylation site. Taken together, these data demonstrate contributions to a similar pathway and support a critical cooperation of PAR2 and TF cytoplasmic domain signaling in promoting angiogenesis in breast cancer development.

Although TF$^{\Delta CT}$ and PAR2$^{-/-}$ mice were remarkably similar in early stages of spontaneous breast cancer progression in the PyMT model, there were differences in these 2 knockout strains in advanced tumors. TF$^{\Delta CT}$ tumor vessel diameters were larger, and PAR2-deficiency of TF$^{\Delta CT}$ mice partially reversed the observed increased vessel diameters. Hypoxia-driven ocular angiogenesis is enhanced in TF$^{\Delta CT}$, but not TF$^{\Delta CT}$/PAR2$^{-/-}$ mice,[23] and a specific inhibitor of TF-VIIa-PAR2 signaling blocks enhanced angiogenesis of TF$^{\Delta CT}$ mice,[21] consistent with a requirement for PAR2 signaling to reveal a host proangiogenic phenotype in TF$^{\Delta CT}$ mice. In addition, TF$^{\Delta CT}$ and TF$^{\Delta CT}$/PAR2$^{-/-}$, but not PAR2$^{-/-}$ mice, had markedly reduced numbers of tumor-associated macrophages (TAMs) in late-stage tumors, indicating that TF cytoplasmic-domain signaling has effects independent of PAR2 in the myeloid compartment to regulate the tumor microenvironment.

The molecular basis for changes in tumor vessel diameters and architecture is poorly understood. One of the regulators of tumor vessel size is the angiopoietin/Tie (Tyrosine kinase with immunoglobulin-like and EGF-like domains) system[37] that is known to be influenced by PAR2 signaling.[38] In the human epidermal growth factor receptor 2 (HER2/neu) transgenic breast cancer model, deficiency in thrombospondin 1 also results in
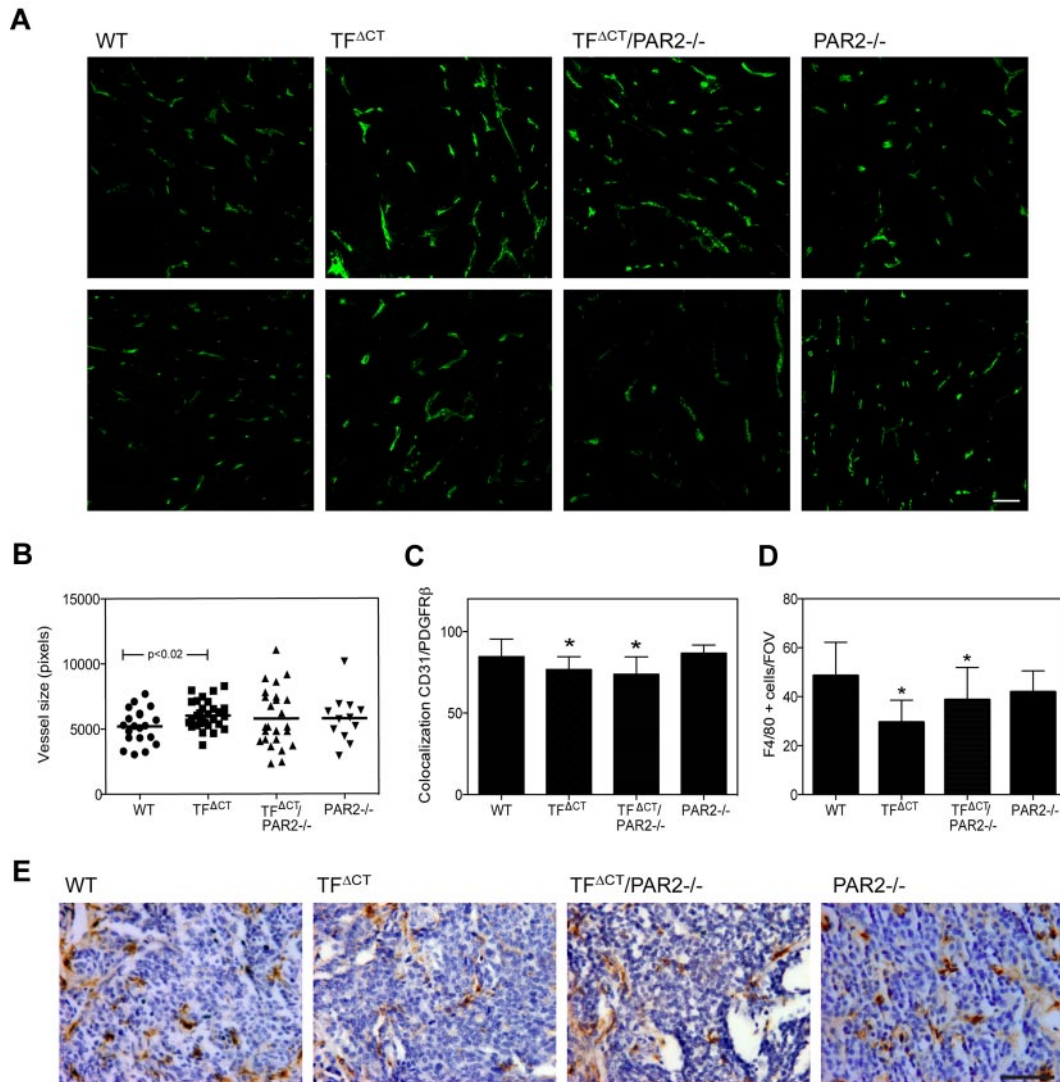
Figure 4. Altered tumor vessel appearance and macrophages recruitment in late stage tumors of TF$^{\Delta CT}$ mice. Tumors from 20-week-old PyMT WT, TF$^{\Delta CT}$, TF$^{\Delta CT}$/PAR2$^{-/-}$, and PAR2$^{-/-}$ mice were stained for CD31 or F4/80. (A) Representative images of CD31 staining in late stage tumors, scale bar 50 μm. (B) CD31 area was quantified using Image Pro plus in 4 different areas of the tumors; n ≥ 5, mean ± SD, P = .02 PyMT WT versus TF$^{\Delta CT}$, t test. (C) Tumor vessels coverage was assessed in PDGFRβ and CD31 costained sections, and colocalization of CD31 and PDFGR-β staining was quantified with Imaris in 4 different areas of at least 3 tumors per genotype (*P < .05 by ANOVA). (D) F4/80-positive cells were counted in 4 different tumor areas of at least 5 tumors per genotype, PyMT TF$^{\Delta CT}$ and TF$^{\Delta CT}$/PAR2$^{-/-}$ different from WT, P < .001 ANOVA. (E) Representative images of F4/80-positive cells (brown staining) in PyMT WT, TF$^{\Delta CT}$, TF$^{\Delta CT}$/PAR2$^{-/-}$, and PAR2$^{-/-}$ tumors; scale bar is 50 μm.

increased vessel size,[39] and thrombospondin is tightly controlled by PAR1 signaling in endothelial cells.[40] Thus, TF-PAR2 signaling in the host compartment may directly or indirectly through crosstalk with host PAR1 signaling determine vessel size.

In the tumor microenvironment, 2 major types of macrophages, M1 and M2, have been described according to the expression of specific markers on their surface and the expression of select cytokines and chemokines. M1 macrophages have a tumoricidal activity and are characterized by the production of tumor necrosis factor (TNF)α and interleukin (IL)–6. In contrast, M2 macrophages have tumor-promoting properties and express vascular endothelial growth factor (VEGF), matrix metalloproteinases (MMPs), and IL-10. Thus, M2-polarized TAMs are crucial for host angiogenic responses.[41] Although TAM numbers were reduced in late stage tumors of TF$^{\Delta CT}$ and TF$^{\Delta CT}$/PAR2$^{-/-}$ mice, this may be compensated by altered signaling in the myeloid compartment that is documented by attenuated adaptive immune responses in TF$^{\Delta CT}$

mice[42] and enhanced microglia activation in neuroinflammation for PAR2$^{-/-}$ mice.[43] A more detailed analysis of TAMs found in TF$^{\Delta CT}$, PAR2$^{-/-}$, and TF$^{\Delta CT}$/PAR2$^{-/-}$ tumors is required to understand the relationship of macrophage phenotypes with vessel architecture in the PyMT model.

The presented data demonstrate a functional overlap of tumor cell TF cytoplasmic domain and PAR2 signaling in supporting the advance of early adenomas to carcinomas that is dependent on the angiogenic switch in early stages of spontaneous breast cancer development in the PyMT model. These data are in excellent agreement with results demonstrating that pharmacological inhibition of direct TF signaling reduced angiogenesis in several tumor models[16,44] and markedly suppressed colon cancer progression in the mouse.[45] Our data also indicate that interruption of TF signaling perturbs angiogenesis and immune cells in the host tumor microenvironment. While species-selective antibodies had provided clear evidence for an important role of tumor cell

signaling,[16] pharmacological inhibition of TF signaling in the host compartment may provide additional benefits to alter tumor angiogenesis. In clinical breast cancer biopsies, TF and PAR2 are up-regulated in invasive cancer relatively to carcinoma in situ and only patients who showed TF phosphorylation suffered a relapse in a small group of prospectively followed, newly diagnosed breast cancers.[27] The data presented here directly show a tumor-promoting role of the TF cytoplasmic domain. Taken together, TF phosphorylation may serve as a marker for increased tumor cell TF signaling and thus prove to be suitable to identify tumors benefiting from therapy with direct inhibitors of TF signaling complexes.

Acknowledgments

Authorship

Contribution: F.S. designed and performed experiments, analyzed data, and wrote the manuscript; H.H.V., A.S., N.Y., and B.M.M. performed experiments and analyzed data; L.C.P. provided critical reagents; and W.R. designed experiments, analyzed data, and wrote the manuscript.

Conflict-of-interest disclosure: The authors declare no competing financial interests.

Correspondence: Wolfram Ruf, Department of Immunology and Microbial Science, The Scripps Research Institute, 10550 North Torrey Pines Rd, SP258, La Jolla, CA 92037; e-mail: ruf@scripps.edu.

References

1. Rickles FR, Patierno S, Fernandez PM. Tissue factor, thrombin, and cancer. *Chest*. 2003;124 (3 suppl):58S-68S.

2. ten Cate H, Falanga A. Overview of the postulated mechanisms linking cancer and thrombosis. *Pathophysiol Haemost Thromb*. 2008;36(3-4): 122-130.

3. Schaffner F, Ruf W. Tissue factor and PAR2 signaling in the tumor microenvironment. *Arterioscler Thromb Vasc Biol*. 2009;29(12):1999-2004.

4. Ruf W, Mueller BM. Thrombin generation and the pathogenesis of cancer. *Semin Thromb Hemost*. 2006;32(suppl 1):61-68.

5. Nierodzik ML, Karpatkin S. Thrombin induces tumor growth, metastasis, and angiogenesis: Evidence for a thrombin-regulated dormant tumor phenotype. *Cancer Cell*. 2006;10(5):355-362.

6. Riewald M, Ruf W. Mechanistic coupling of protease signaling and initiation of coagulation by tissue factor. *Proc Natl Acad Sci U S A*. 2001; 98(14):7742-7747.

7. Liu Y, Mueller BM. Protease-activated receptor-2 regulates vascular endothelial growth factor expression in MDA-MB-231 cells via MAPK pathways. *Biochem Biophys Res Commun*. 2006; 344(4):1263-1270.

8. Albrektsen T, Sorensen BB, Hjortoe GM, et al. Transcriptional program induced by factor VIIa-tissue factor, PAR1 and PAR2 in MDA-MB-231 cells. *J Thromb Haemost*. 2007;5(8):1588-1597.

9. Hjortoe GM, Petersen LC, Albrektsen T, et al. Tissue factor-factor VIIa specific up-regulation of IL-8 expression in MDA-MB-231 cells is mediated via PAR-2 and results in increased cell migration. *Blood*. 2004;103(8):3029-3037.

10. Kumar P, Lau CS, Mathur M, Wang P, DeFea KA. Differential effects of beta-arrestins on the internalization, desensitization and ERK1/2 activation downstream of protease activated receptor-2. *Am J Physiol Cell Physiol*. 2007;293(1):C346-C357.

11. Zoudilova M, Kumar P, Ge L, et al. Beta-arrestin-dependent regulation of the cofilin pathway downstream of protease-activated receptor-2. *J Biol Chem*. 2007;282(28):20634-20646.

12. Morris DR, Ding Y, Ricks TK et al. Protease-activated receptor-2 is essential for factor VIIa and Xa-induced signaling, migration, and invasion of breast cancer cells. *Cancer Res*. 2006;66(1):307-314.

13. Ge L, Shenoy SK, Lefkowitz RJ, DeFea K. Constitutive protease-activated receptor-2-mediated migration of MDA MB-231 breast cancer cells requires both beta-arrestin-1 and -2. *J Biol Chem*. 2004;279(53):55419-55424.

14. Wang P, DeFea KA. Protease-activated receptor-2 simultaneously directs beta-arrestin-1-dependent inhibition and Galphaq-dependent activation of phosphatidylinositol 3-kinase. *Biochemistry*. 2006;45(31):9374-9385.

15. Dorfleutner A, Hintermann E, Tarui T, Takada Y, Ruf W. Crosstalk of integrin alpha3beta1 and tissue factor in cell migration. *Mol Biol Cell*. 2004; 15(10):4416-4425.

16. Versteeg HH, Schaffner F, Kerver M, et al. Inhibition of tissue factor signaling suppresses tumor growth. *Blood*. 2008;111(1):190-199.

17. Even-Ram S, Uziely B, Cohen P, et al. Thrombin receptor overexpression in malignant and physiological invasion processes. *Nature Med*. 1998; 4(8):909-914.

18. Booden MA, Eckert LB, Der CJ, Trejo J. Persistent signaling by dysregulated thrombin receptor trafficking promotes breast carcinoma cell invasion. *Mol Cell Biol*. 2004;24(5):1990-1999.

19. Versteeg HH, Schaffner F, Kerver M, et al. Protease activated receptor (PAR)2, but not PAR1 signaling promotes the development of mammary adenocarcinoma in PyMT mice. *Cancer Res*. 2008;68(17):7219-7227.

20. Lin EY, Jones JG, Li P, et al. Progression to malignancy in the polyoma middle T oncoprotein mouse breast cancer model provides a reliable model for human diseases. *Am J Pathol*. 2003; 163(5):2113-2126.

21. Uusitalo-Jarvinen H, Kurokawa T, Mueller BM, et al. Role of protease activated receptor 1 and 2 signaling in hypoxia-induced angiogenesis. *Arterioscler Thromb Vasc Biol*. 2007;27(6):1456-1462.

22. Yu J, May L, Milsom C, et al. Contribution of host-derived tissue factor to tumor neovascularization. *Arterioscler Thromb Vasc Biol*. 2008;28(11):1975-1981.

23. Belting M, Dorrell MI, Sandgren S, et al. Regulation of angiogenesis by tissue factor cytoplasmic domain signaling. *Nature Med*. 2004;10(5):502-509.

24. Abe K, Shoji M, Chen J, et al. Regulation of vascular endothelial growth factor production and angiogenesis by the cytoplasmic tail of tissue factor. *Proc Natl Acad Sci U S A*. 1999;96(15):8663-8668.

25. Mueller BM, Ruf W. Requirement for binding of catalytically active factor VIIa in tissue factor dependent experimental metastasis. *J Clin Invest*. 1998;101(7):1372-1378.

26. Bromberg ME, Konigsberg WH, Madison JF, Pawashe A, Garen A. Tissue factor promotes melanoma metastasis by a pathway independent of blood coagulation. *Proc Natl Acad Sci U S A*. 1995;92(18):8205-8209.

27. Ryden L, Grabau D, Schaffner F, et al. Evidence for tissue factor phosphorylation and its correlation with protease activated receptor expression and the prognosis of primary breast cancer. *Int J Cancer*. 2010;126(10):2330-2340.

28. Ahamed J, Ruf W. Protease-activated receptor 2-dependent phosphorylation of the tissue factor cytoplasmic domain. *J Biol Chem*. 2004;279(22): 23038-23044.

29. DeFea KA, Zalevsky J, Thoma MS, et al. beta-Arrestin-dependent endocyrosis of protein-ase-activated receptor 2 is required for intracellular targeting of activated ERK1/2. *J Cell Biol*. 2000;148(6):1267-1281.

30. Petersen LC, Norby PL, Branner S, et al. Characterization of recombinant murine factor VIIa and recombinant murine tissue factor: a human-murine species compatibility study. *Thromb Res*. 2005;116(1):75-85.

31. Zhou Q, Kiosses WB, Liu J, Schimmel P. Tumor endothelial cell tube formation model for determining anti-angiogenic activity of a tRNA synthetase cytokine. *Methods*. 2008;44(2):190-195.

32. Ricks TK, Trejo J. Phosphorylation of protease-activated receptor-2 differentially regulates desensitization and internalization. *J Biol Chem*. 2009;284(49):34444-34457.

33. Palumbo JS, Talmage KE, Massari JV, et al. Tumor cell-associated tissue factor and circulating hemostatic factors cooperate to increase metastatic potential through natural killer cell-dependent and -independent mechanisms. *Blood*. 2007;110(1):133-141.

34. Ahamed J, Niessen F, Kurokawa T, et al. Regulation of macrophage procoagulant responses by the tissue factor cytoplasmic domain in endotoxemia. *Blood*. 2007;109(12):5251-5259.

35. Cunningham MA, Romas P, Hutchinson P, Holdsworth SR, Tipping PG. Tissue factor and factor VIIa receptor/ligand interactions induce proinflammatory effects in macrophages. *Blood*. 1999; 94(10):3413-3420.

36. Rak J, Yu JL, Luyendyk J, Mackman N. Oncogenes, trousseau syndrome, and cancer-related changes in the coagulome of mice and humans. *Cancer Res*. 2006;66(22):10643-10646.

37. Li Z, Huang H, Boland P, et al. Embryonic stem cell tumor model reveals role of vascular endothelial receptor tyrosine phosphatase in regulating Tie2 pathway in tumor angiogenesis. *Proc Natl Acad Sci U S A*. 2009;106(52):22399-22404.

38. Zhu T, Sennlaub F, Beauchamp MH, et al. Proangiogenic effects of protease-activated receptor

2 are tumor necrosis factor-alpha and consecutively Tie2 dependent. *Arterioscler Thromb Vasc Biol.* 2006;26(4):744-750.

39. Rodriguez-Manzaneque JC, Lane TF, Ortega MA, et al. Thrombospondin-1 suppresses spontaneous tumor growth and inhibits activation of matrix metalloproteinase-9 and mobilization of vascular endothelial growth factor. *Proc Natl Acad Sci U S A.* 2001;98(22):12485-12490.

40. Riewald M, Ruf W. Protease-activated receptor-1 signaling by activated protein C in cytokine-perturbed endothelial cells is distinct from thrombin signaling. *J Biol Chem.* 2005;280(20):19808-19814.

41. Qian BZ, Pollard JW. Macrophage diversity enhances tumor progression and metastasis. *Cell.* 2010;141(1):39-51.

42. Yang YH, Hall P, Milenkovski G, et al. Reduction in arthritis severity and modulation of immune function in tissue factor cytoplasmic domain mutant mice. *Am J Pathol.* 2004;164(1):109-117.

43. Noorbakhsh F, Tsutsui S, Vergnolle N, et al. Proteinase-activated receptor 2 modulates neuroinflammation in experimental autoimmune encephalomyelitis and multiple sclerosis. *J Exp Med.* 2006;203(2):425-435.

44. Hembrough TA, Swartz GM, Papathanassiu A, et al. Tissue factor/factor VIIa inhibitors block angiogenesis and tumor growth through a nonhemostatic mechanism. *Cancer Res.* 2003;63(11): 2997-3000.

45. Zhao J, Aguilar G, Palencia S, Newton E, Abo A. rNAPc2 inhibits colorectal cancer in mice through tissue factor. *Clin Cancer Res.* 2009;15(1):208-216.